Chemosphere 286 (2022) 131770

Contents lists available at ScienceDirect

Chemosphere

journal homepage: www.elsevier.com/locate/chemosphere

Removal of chlortetracycline from water using spent tea leaves-based biochar as adsorption-enhanced persulfate activator

Yi-Ping Chen [a,*], Chao-Hong Zheng [a], Yao-Yi Huang [a], Yi-Ren Chen [b]

[a] College of Resources and Environment, Quanzhou Normal University, 398 Donghai Road, Quanzhou, 362000, China
[b] State Key Laboratory of Luminescence and Applications, Changchun Institute of Optics, Fine Mechanics and Physics, Chinese Academy of Sciences, Changchun, 130033, China

HIGHLIGHTS

- The STLB as a sustainable adsorption-enhanced activator was prepared.
- CTC was effectively removed by adsorption-promoted PS-AOP in a broad pH range.
- CTC adsorption on STLB was good for the subsequent in-situ degradation.
- CTC degradation was due to the reactive species including $^{\bullet}SO_4^-$, $^{\bullet}OH$, and $^1O_2$.
- This study provided a new strategy of treating waste with spent tea leaves.

GRAPHICAL ABSTRACT

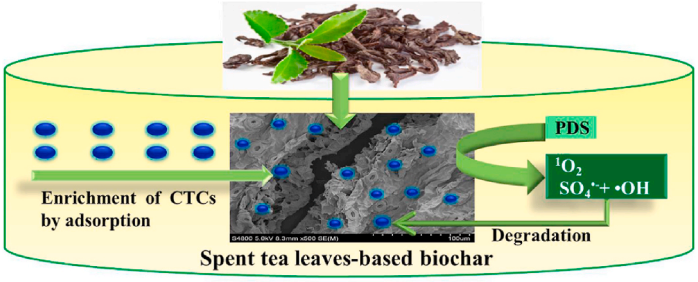

ARTICLE INFO

Handling Editor: Chang Min Park

Keywords:
Spent tea leaves
Adsorption
Persulfate
Chlortetracycline
Reaction mechanism

ABSTRACT

Antibiotic compounds have caused serious environmental concerns. In this study, we developed an effective technology for treatment of chlortetracycline (CTC), a widely used antibiotic compound. A natural heteroatom-doped spent tea leaves-based biochar (STLB) with excellent adsorption and catalytic property was prepared by simple thermal treatment. An adsorption-promoted persulfate-based advanced oxidation process (PS-AOP) using STLB was studied for CTC removal. The results showed that the as-prepared STLB presented favorable adsorption affinity towards CTC with the maximum adsorption capacity of 627 mg g^{-1}. Meanwhile, CTC enriched on the surface of STLB was good for in-situ decomposition of CTC and nearly 97.4 % of CTC was removed within 30 min of pre-adsorption and 60 min of subsequent degradation. The STLB had excellent recyclability and wide pH tolerance range of 3.0–9.0 in combined pre-adsorption and PS-AOP. Reactive oxygen species analysis confirmed that CTC degradation was mainly due to non-radical (singlet oxygen, $^1O_2$) and radicals ($SO_4^{\bullet-}$ and $^{\bullet}OH$). This study suggests that STLB is a promising adsorption-enhanced PS activator for the treatment of refractory wastewater and also provides a strategy of waste control by spent tea leaves.

1. Introduction

Chlortetracycline (CTC), as a widely used antibiotic, has been frequently detected in water bodies and wastewater treatment plants at concentrations ranging from 18.1 ng L^{-1} to 1.8 mg L^{-1} (Ding et al., 2017; Hou et al., 2016). It holds an increasing threat to ecological

* Corresponding author.
E-mail address: chenyiping2005@qztc.edu.cn (Y.-P. Chen).

https://doi.org/10.1016/j.chemosphere.2021.131770
Received 3 June 2021; Received in revised form 28 July 2021; Accepted 31 July 2021
Available online 2 August 2021

environment and human health even at trace levels of exposure (W. Li et al., 2020; Ouda et al., 2021). Thus, it's urgent to develop efficient methods for the removal of residual antibiotics from water.

Recently, persulfate-based advanced oxidation process (PS-AOP) has exhibited great potential in removing refractory organic contaminants including antibiotics from aquatic environment (Oh et al., 2016). Compared with the usual Fenton-based advanced oxidation process, PS-AOP with the introduced sulfate radicals and non-radical active complexes manifests better selectivity, higher mineralization potential, and wider pH adaptability. Moreover, persulfates (PS), involving peroxymonosulfate (PMS) and peroxodisulfate (PDS), are lower cost and better chemical stability during transportation and storage than hydrogen peroxide (H_2O_2).

Various studies have proved that metal-free carbon materials are highly effective for PS activation (Zhao et al., 2017). Compared to metal-based catalysts, metal-free catalysts have the merits of good stability, provide an effective solution to undesirable metal leaching problem, and avoid massive formation of iron sludge during catalytic degradation (Yu et al., 2020). But, among the metal-free catalysts, the synthesis of some emerging carbon materials, such as graphene oxides, is complicated with harsh conditions and low yields. In comparison, the biochar generated from natural and renewable bio-resource is more sustainable (Wan et al., 2020).

As a popular beverage, about 20 billion cups of tea are drunk daily in the world (Razmovski et al., 2008). After drinking, approximately 5 million of spent tea leaves will be generated per year according to the statistically data (Fan et al., 2016). This will inevitably cause great waste of resources and bring a series of environment and ecological problems (Bsoul et al., 2021). Compared with other precursors of biochar such as wood, tea leaves contain about 3.34 mg kg^{-1} iron (Karak et al., 2017; Mandal et al., 2020), which is firmly fixed in the natural leaf tissue. So that it is not easy to cause metal leaching during the PS activation by iron. Besides, the tea leaves are rich in some elements involving 0.4 mg kg^{-1} sodium and 3.4 mg kg^{-1} nitrogen (Karak et al., 2017; Mandal et al., 2020). The surface of spent tea leaves is still covered with many open stomata and functional groups (Mandal et al., 2020). The heteroatom-doped porous biochar will be made without additional doping and immobilization (Wan et al., 2020), which is good for activating PS to generate some stronger reactive oxygen species such as sulfate radical ($SO_4^{-\bullet}$) and singlet oxygen ($^1O_2$) (Hameed et al., 2009; Duan et al., 2018). Meanwhile, spent tea leaves are also good porous bio-adsorbents with multi-layer physical adsorption capacity (Ng et al., 2013; Qalyoubi et al., 2021), which is conducive to the enrichment of trace pollutants in water for intricate microporous structure on the inner surface of tea-leaves and porous reticular structure on the surface of tea-leaves. Conversely, the catalytically generated active oxygen species rapidly degrade the adsorbed pollutant in the presence of PS, accelerating the regeneration of adsorption active sites and the continuous enrichment of residual pollutant (Gan et al., 2018). The adsorption and catalytic degradation will promote each other to achieve better removal efficiency. Thus, spent tea leaves-based biochar (STLB), as a promising sustainable adsorption-enhanced persulfate activator for the PS-AOP system, will have inestimable potential in removing trace pollutants from water owing to highly abundant resources, low cost, good safety, and enhanced removal behavior (Peiris et al., 2017).

Herein, a biomass-derived metal-free catalyst with strong adsorption capacity was synthetized using the low-cost spent tea leave as carbon source. Then, the adsorption-promoted PS activation behavior of as-prepared STLB for CTC removal was systematically studied. This study aims to construct an adsorption-enhanced PS-AOP for the efficient removal of low-level antibiotics in water, and provide a new strategy of treating waste with bio-waste as well as turning spent tea leave into treasure.

2. Experimental section

2.1. Chemicals and materials

Nitric acid (HNO_3), 5,5-dimethyl-1-pyrroline Noxide (DMPO, 98 %), 2,2,6,6-tetramethylpiperidine (TEMP, >99 %), sodium dihydrogenphosphate (NaH_2PO_4), ethanol (EtOH), *tert*-butyl alcohol (TBA) and sodium azide (NaN_3) were provided by Sinopharm Chemical Reagent Co. Ltd. (Shanghai, China). Chlortetracycline (CTC, purity ≥98 %) was purchased from the Sigma-Aldrich Corporation. All of the above chemicals were of analytical grade and used without further purification. Acetonitrile was of HPLC grade and supplied from Merck (Darmstadt, Germany).

The oolong tea leaves, which were obtained from Richun Tea Co, Ltd. (Fujian, China), were repeatedly washed in boiling water until the filtered water was clear. And then the spent tea leaves were dried in oven at 60 °C for further use.

2.2. Synthesis of spent tea leaves-based biochar

The STLB was fabricated by simple thermal treatment. First, the spent tea leaves were pre-oxidation in air environment at 250 °C for 0.5 h (heating rate was 5 °C min^{-1}). During the pre-oxidation stage, the enhancement of cross-linking reactions among oxygen functional groups would be conducive to the increase of subsequent carbonization yield and the broader distribution of micropore (Worasuwannarak et al., 2002). Then, the treated spent tea leaves were placed in a tubular electrical furnace and carbonized at 500 °C for 1 h in N_2 atmosphere (heating rate was 5 °C min^{-1}) to form STLB. After that, the obtained biochar was treated with 1 M HCl, rinsed with deionized water until the pH value reached about 6.0, and dried in oven at 60 °C. Finally, the dried STLBs were grinded and sieved to their particle sizes ranging from 250 to 800 μm for later use.

2.3. Characterization

The morphology of STLB was observed using a Hitachi S-4800 field emission scanning electron microscope (SEM, Japan). The Brunauer-Emmett-Teller (BET) surface area and pore size distribution of samples were determined with a Micromeritics ASAP2020 M + C apparatus (Georgia) by N_2 adsorption-desorption isotherms at 77 K. The crystal phase of STLB was characterized by a D/max-2550 VB+/PC X-ray diffractometer (XRD, Rigaku, Japan). The surface functional groups were analyzed by a Nicolet 5700 fourier transform infrared spectrometer (FTIR, Thermo Corp, USA). The elemental composition was studied by a PerkinElmer PHI-5300 ESCA X-ray photoelectron spectroscopy (XPS, Philadelphia, USA). The STLB was further burned at 250 °C under O_2 atmosphere and then the residual powder was dissolved in acid. The concentration of iron ion was measured by an Optima 8000 inductively coupled plasma atomic emission spectrometry (ICP-AES, USA).

2.4. Adsorption performance

To evaluate the enrichment effect of CTC on STLB, batch adsorption isotherms experiments were first performed in 250 mL glass bottles for a series of CTC solutions (50–500 mg L^{-1}). The STLB (0.1 g L^{-1}) was added into CTC solution and shaken at 150 rpm. The glass bottles were shaken for 200 min to ensure the adsorption equilibrium. Then the equilibrium solutions were filtered through 0.45 μm syringe filters and analyzed by HPLC. Besides, both Langmuir (Eq. S1) and Freundlich (Eq. S2) models (Kakavandi et al., 2014) were further used to analyze adsorption isotherm property.

The adsorption kinetics experiment was conducted with the same operating condition as the adsorption equilibrium study. The STLB (0.1 g L^{-1}) was added into 200 mL of 50 mg L^{-1} CTC solution. At given time intervals, 1.5 mL of sample was immediately filtered using 0.45 μm

syringe filter and the residual CTC concentration at different time was analyzed by HPLC. In addition, three commonly used kinetics models, including pseudo-first-order (Eq. S3), pseudo-second-order (Eq. S4), and Weber-Morris kinetics models (Eq. S5) (Chen et al., 2019), were further applied to interpret kinetics data.

The point of zero charge pH (pH_{pzc}) of STLB and chemical species distribution of CTC at different pH were determined using the immersion technique (Liu et al., 2015). Briefly, the electrolyte (200 mL of 0.05 M NaCl) solutions were adjusted to initial pH values of 3, 4, 5, 6, 7, 8, 9, or 10 using 0.1 M H_2SO_4 or 0.1 M NaOH, respectively. The STLB (0.1 g L^{-1}) was added into each solution and shaken at 25 °C until the equilibrium pH was reached. And then the difference between the final and initial pH (ΔpH) was recorded. The initial pH at which ΔpH equaled to zero was considered to be the pH_{pzc} of STLB.

2.5. Adsorption-promoted degradation performances

The adsorption-promoted degradation experiment was conducted in a batch reactor containing 200 mL of 50 mg L^{-1} CTC solution. The whole experiment operated in a batch mode could be divided into two stages: the pre-adsorption stage and the PS-AOP degradation stage. During the pre-adsorption process, 0.1 g L^{-1} of STLB was first added into CTC solution and placed on a shaker to enrich and condense CTC molecules from water. After that, the PDS (1 g L^{-1}) was introduced into the reaction system to initiate PS-AOP. PDS would be simultaneously catalyzed by the unveiled activation sites on STLB to produce some active species such as $SO_4^{-\bullet}$ and $^1O_2$, which led to the CTC degradation and the regeneration of STLB. At given time intervals, 1.5 mL of sample was immediately filtered using 0.45 μm syringe filter, and then mixed with 1.0 mL methanol to terminate the oxidation. The residual CTC concentration at different time was measured by HPLC.

In the pH-dependent study, solution pH was adjusted to 3, 7 and 9 using 0.1 M H_2SO_4 or 0.1 M NaOH. For the reusability tests, used STLB was washed with distilled water and then dried at 60 °C. Other experimental conditions remained the same for the subsequent runs.

2.6. Analytic methods

The CTC concentrations were monitored by a Hitachi Model L-6200 HPLC system (Japan) equipped with a Beckman ODS C18 column (5 μm, 250 mm × 4.6 mm) at λ = 355 nm. The mobile phase was a mixture of acetonitrile and water containing 0.01 M NaH_2PO_4 (25:75, v/v). The injection volume was 10 μL and the flow rate was set at 1.0 mL min^{-1}. Electron paramagnetic resonance (EPR) analysis with DMPO and TEMP as trapping agents was conducted on a Bruker EMX-E8/2.7 spectrometer (Germany). To further distinguish the roles of generated reactive oxygen species, 0.5 M EtOH, 0.5 M TBA, or 0.5 M NaN_3, were added into the reaction systems as radical scavengers, respectively. Total organic carbon (TOC) was tested by a Shimadzu TOC-VCPH analyzer (Japan).

3. Results and discussion

3.1. Characterization of spent tea leaves-based biochar

The morphologies of spent tea leaves before and after heat treatment were characterized by SEM. As illustrated in Fig. 1a, before thermal treatment, the spent tea leaves exhibited rough surface with many obvious cracks and open stomata. Fig. 1b demonstrated SEM image of STLB synthesized by thermal reaction. It is obvious that the stomata in spent tea leaves opened wider and lots of holes were completely formed due to dehydration after thermal treatment. A tunnel porous network structure was distributed on the inner and outer surface of the STLB, which would be good for promoting adsorption and catalysis (Yu et al., 2021). The result of X-ray diffractometer (XRD) analysis was described in detail in Text S1, which also proved that the spent tea leaves were mainly converted to amorphous carbon after heat treatment.

The porosity properties of STLB were analyzed by N_2 adsorption-desorption isotherms (Fig. 2a). The result showed that specific surface area of as-prepared material was 503 m^2 g^{-1}, which far exceeded that of other biochar such as sludge biochar, wood biochar, and magnetic pine sawdust biochar (Yu et al., 2020). According to the IUPAC classification, the N_2 adsorption-desorption curve demonstrated a type Ⅳ isotherm with a rapid uptake in the low-pressure region, followed by a moderate increase under relatively intermediate pressure and a steep increase in the high-pressure region. This highlights the formation of a hierarchical pore architecture involving micropores (<2 nm), mesopores (2–50 nm), and even macropores (>50 nm), which was in accordance with the corresponding pore size distribution based on a Barrett-Joyner-Halenda equation (inset). The STLB had a broad pore size distribution with irregular arrangement, where micropore, mesopore and macropore coexist. The average pore diameter was about 4.07 nm. The pore volume of as-prepared material was 0.25 cm^3 g^{-1} and the micropore volume was 0.20 cm^3 g^{-1}. Herein, microporosity and mesoporosity would play important roles in creating more active sites for adsorption and catalysis, enhancing the CTC removal. Meanwhile, macroporosity would be helpful for low-resistant diffusion of generated reactive oxygen species and subsequent desorption and degradation of CTC.

The chemical state and elemental composition of STLB were analyzed by XPS (Fig. 2b–f). As presented in Fig. 2b, the wide-survey XPS spectrum of as-prepared material showed four obvious characteristic peaks of S 2p (168.84 eV, 3.17 at.%), C 1s (284.78 eV, 54.07 at.%), N 1s (400.34 eV, 3.89 at.%) and O 1s (545.78 eV, 38.87 at.%). The XPS spectrum for S 2p (Fig. 2c) could be deconvoluted into two types of oxidized S species, namely sulfate (170.1 eV) and sulfonate functional groups (168.8 eV) (Wang et al., 2015). The inherent S in the spent tea leaves could promote the formation of more Louis acid-base sites in the biochar, which would enhance the PDS activation (Wang et al., 2019). The C1s spectrum could be subdivided into four individual peaks (Fig. 2d). The main peaks at 286.5 eV, 284.8 eV, 285.1 eV and 289.0 eV could be assigned to epoxy C–*O*–C, C═C, C–O, and C═O, respectively (Zhu et al., 2019). The N 1s spectrum (Fig. 2e) was assigned to three

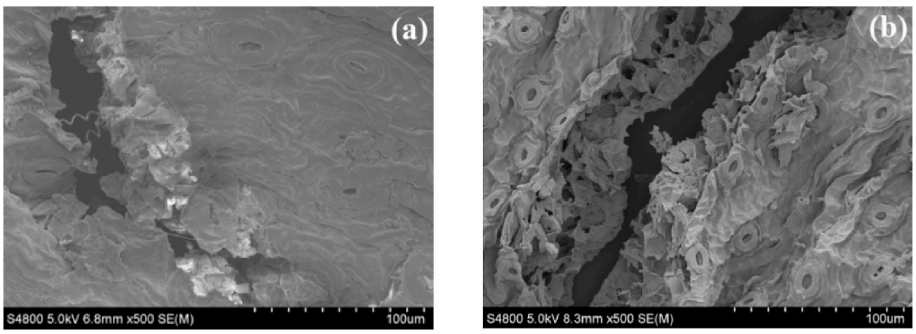

Fig. 1. SEM images of (a) spent tea leaves before heat treatment and (b) STLB.

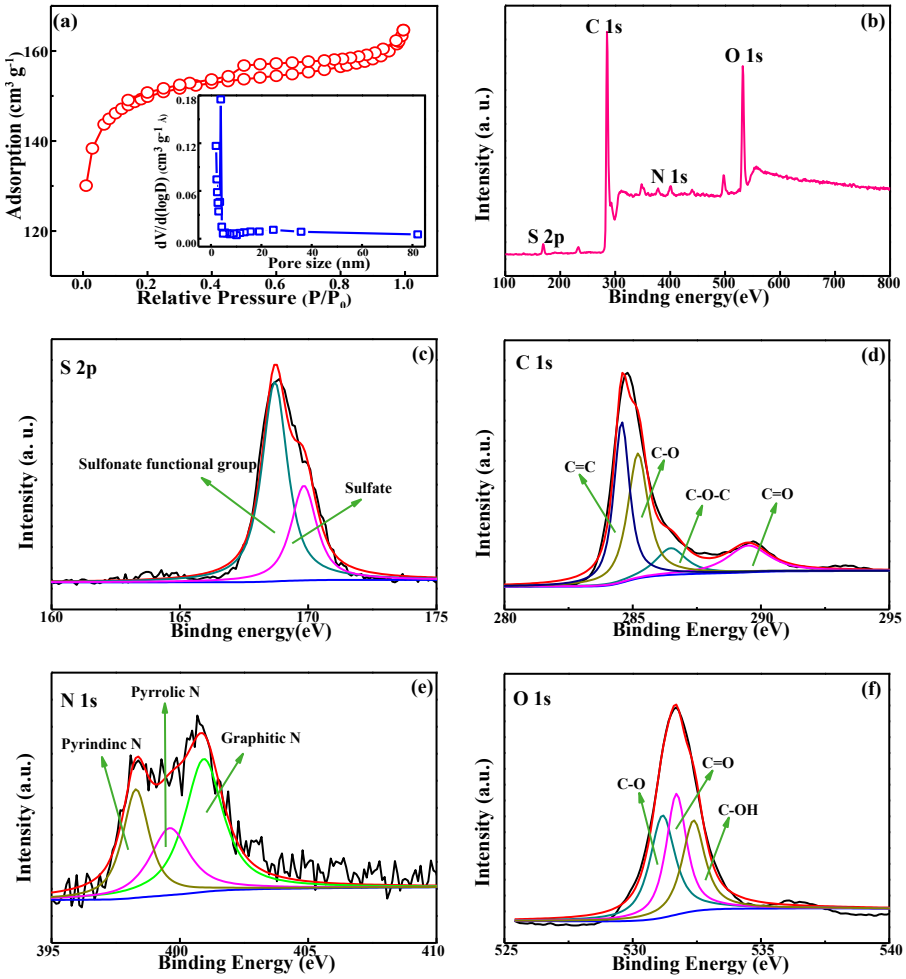

Fig. 2. (a) Nitrogen adsorption-desorption isotherms of STLB with the corresponding pore sizes distribution (inset); (b) XPS survey of STLB; (c) High-resolution XPS of S 2p; (d) High-resolution XPS of C 1s; (e) High-resolution XPS of N 1s; (f) High-resolution XPS of O 1s.

types: pyridinic N at 398.3 eV, pyrrolic N at 399.9 eV, and graphitic N at 400.7 eV (Jiang et al., 2018). The existence of heteroatoms such as N could break the chemical inertness of original carbon layer, produce more surface defects, and provide more reaction sites for PDS activation (Wang et al., 2020). As shown in Fig. 2f, the O 1s high resolution spectra could be decomposed into three peaks, corresponding to C–OH (533.0 eV), C═O (532.3 eV), and C–O (531.2 eV) (Deng et al., 2019). Besides, due to the low content of iron in STLB, it could not be detected by XPS. But the Fe concentration of STLB measured by ICP-AES was 250.9 mg kg^{-1}. These oxygen functional groups and trace amounts of iron would present high redox potential and facilitate electron transfer from the STLB catalyst to PDS (Jiang et al., 2018).

3.2. CTC removal by the spent tea leaves-based biochar

During CTC removal in PS-AOP, the STLB might act as both an adsorbent and a catalyst. Moreover, CTC adsorption on the STLB would have a positive influence on the subsequent degradation. Thus, the adsorption behavior of as-prepared biochar for CTC removal was first investigated.

3.2.1. CTC adsorption on the spent tea leaves-based biochar activator

3.2.1.1. Adsorption isotherm. The adsorption isotherm performance of CTC on the STLB was evaluated and Langmuir and Freundlich model fits were shown in Fig. 3a. The results indicated that the experimental data was better fitted to the Freundlich model, meaning that the whole adsorption process might belong to a possible multi-layer adsorption with non-uniform distribution of adsorption affinities over the surfaces of STLB. The n value got from the Freundlich model is an indicator of isotherm nonlinearity as well as the heterogeneity of sorption sites. Obviously, the n value obtained for the adsorption system was found to be well above 1, indicating the favorability of the CTC adsorption under the experimental conditions. And the active sites of STLB surface were heterogeneous for CTC binding (Kumar et al., 2016). Besides, the maximum adsorption capacity of as-prepared material obtained from the Langmuir model was 627 mg g^{-1}.

3.2.1.2. Adsorption kinetics. The adsorption kinetic performance of CTC on STLB was also evaluated using pseudo-first-order, pseudo-second-order, and Weber-Morris kinetics models in Fig. 3b & c. As shown, CTC adsorption behavior on the STLB exhibited a rapid phase at the beginning followed by a gradually slower increase until the equilibrium was achieved within 90 min.

According to the fitting results of both pseudo-first-order and pseudo-second-order models (Fig. 3b), the pseudo-first-order model was more suitable to describe the adsorption process, implying that CTC adsorption on the STLB was controlled by a diffusion step (Ng et al., 2013) and the hierarchical pore structure was just favorable for the transport and diffusion of CTC molecules in water (Yu et al., 2021). And then the Weber-Morris model (Fig. 3c) was used to identify the diffusion mechanism. The results showed that the whole adsorption process might

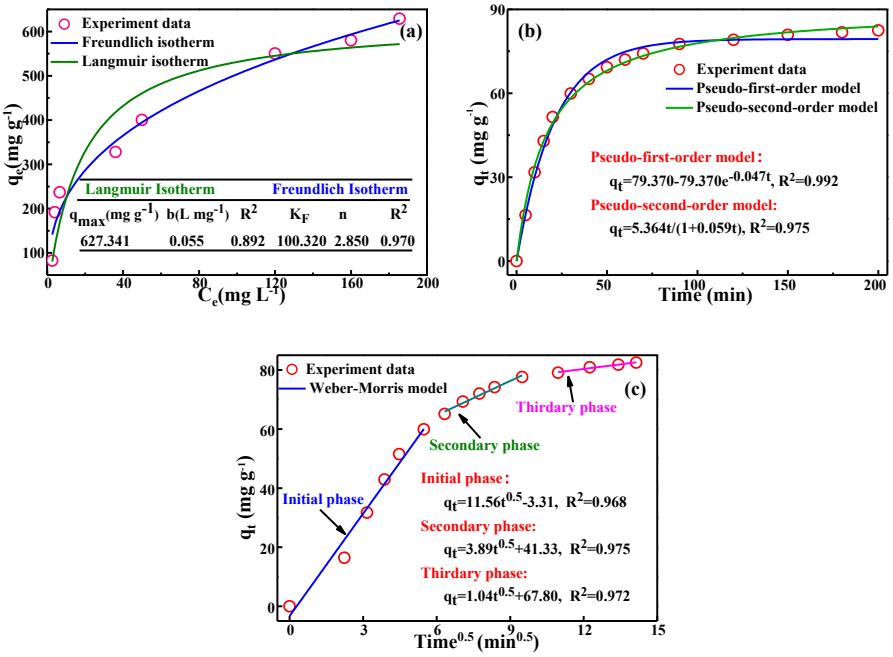

Fig. 3. (a) Adsorption isotherm of CTC on the STLB. Experimental conditions: [STLB] = 0.1 g L^{-1}; [CTC] = 50–500 mg L^{-1}; initial pH = 6.0. (b) Adsorption kinetic curves of CTC fitted with Pseudo-first-order and Pseudo-second-order models; (c) Adsorption kinetic curves of CTC fitted with Weber-Morris model. Experimental conditions: [STLB] = 0.1 g L^{-1}; [CTC] = 50 mg L^{-1}; initial pH = 6.0.

be divided into three stages: (1) External diffusion (0–30 min) where CTC was diffused from bulk solution to external surface of the STLB. (2) Intra-particle diffusion (30–90 min) where CTC was transferred from the surface of STLB into its internal pores. (3) Final equilibrium stage (≥90 min) where intra-particle diffusion began to slow down owing to extremely low CTC concentration left in the solution. The linear plot didn't pass through the origin, suggesting that the intra-particle diffusion wasn't the dominating mechanism for CTC adsorption on synthesized biochar (Chen et al., 2019). Over 75 % of the equilibrium level had been achieved after 30 min, and external adsorption was more conducive to the following desorption and degradation of CTC on STLB. Therefore, 30 min were chosen as the optimum time of CTC pre-adsorption in the subsequent removal experiments.

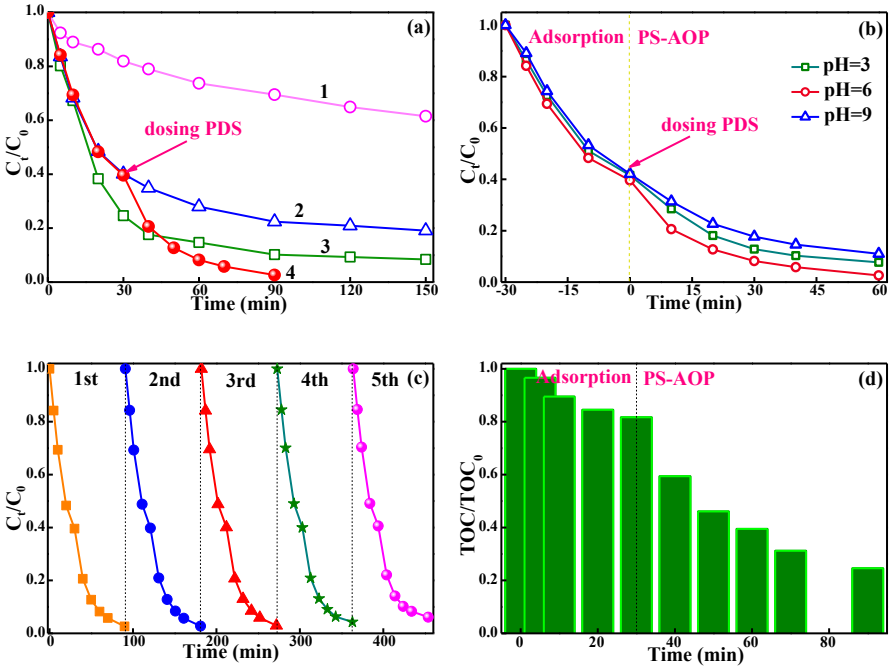

Fig. 4. (a) CTC removal in different systems: (1) oxidation by PDS alone; (2) adsorption using the STLB; (3) PDS activated by the STLB; (4) combined pre-adsorption and PS-AOP derived by the STLB. (b) Effect of initial pH value on the performance of CTC removal, (c) Recyclability of the STLB for CTC removal, and (d) TOC removal in combined pre-adsorption and PS-AOP. Experimental conditions: [STLB] = 0.1 g L^{-1}; [CTC] = 50 mg L^{-1}; [PDS] = 1 g L^{-1}; initial pH = 6.0.

3.2.2. Combined adsorption and degradation performance for CTC removal

3.2.2.1. Adsorption-enhanced catalytic degradation performance. To identify the contribution of adsorption on the subsequent catalytic degradation, the removal efficiencies of CTC in various processes were compared, respectively. As illustrated in Fig. 4a, obviously, only adsorption happened in the presence of STLB and the adsorption resulted in about 77.6 % removal of CTC within 90 min. With the PDS alone, only 30.5 % of CTC was degraded after 90 min. This result indicated that PDS has limited oxidation capacity and CTC cannot be effectively oxidized by PDS without the involvement of catalysts. When both STLB and PDS were present in the system, CTC removal efficiency increased to 89.8 % in 90 min. The result showed that the STLB was effective in activating PDS for the CTC degradation and the oxidizing ability of some reactive oxygen species generated during activation might be much stronger than that of PDS (Liu et al., 2020). Clearly, the best removal performance was achieved in combined pre-adsorption and PS-AOP. An accelerated removal rate was observed and nearly 97.4 % of CTC was removed in 90 min. This might be attributed to that the CTC molecules enriched on the surface of STLB provided higher driving force for their subsequent degradation. In turn, the CTC degradation from the surface of STLB facilitated the sustainable adsorption. The synergistic effect of adsorption coupled with catalysis based on STLB finally resulted in the easy removal of CTC.

The tolerance of pH value has important impact on the performance of adsorption-enhanced PS activation and the practical application of STLB in the wastewater treatment. Thus, the influence of initial solution pH on the CTC removal was investigated at pH 3.0, 6.0 and 9.0, respectively. As illustrated in Fig. 4b, over 92.3 %, 97.4 %, and 89.0 % of CTC were removed within 30 min of pre-adsorption and 60 min of subsequent catalytic degradation at the initial pH of 3.0, 6.0, and 9.0, respectively. The results demonstrated that STLB had high CTC removal efficiency over a wide pH range of 3.0–9.0. By contrast, the CTC removal rate at pH 6.0 was slightly higher than that at pH values of 3.0 and 9.0. This phenomenon might be explained by the fact that pH value had a relatively obvious effect on the performance of adsorption and the generation of free radicals during the CTC removal. Obviously, with the increase of pH value, the adsorption speed increased at first and then decreased gradually (Peiris et al., 2017). The adsorption efficiency was best at pH 6 and this result was basically consistent with the analysis of pH_{pzc} (Text S2 and Fig. S2). Besides, the amount of reactive oxygen species produced under different pH conditions directly influenced the CTC degradation. Compared with alkaline condition, more reactive oxygen species would be generated under acid condition. But some free radicals might be wasted by side reactions (Eq. (1) and (2)) at pH = 3 (Li et al., 2020). Under alkaline condition, SO_4^{-}• could also be transformed to •OH (Eq. (3) and (4)), which had obviously weaker oxidizing power (Yu et al., 2021)).

$$SO_4^{\cdot-} + H^+ + e^- \rightarrow HSO_4^- \quad (1)$$

$$\cdot OH + H^+ + e^- \rightarrow H_2O \quad (2)$$

$$SO_4^{\cdot-} + OH^- \rightarrow \cdot OH + SO_4^{2-} \quad (3)$$

$$SO_4^{\cdot-} + H_2O \rightarrow \cdot OH + H^+ + SO_4^{2-} \quad (4)$$

In order to further explore the recyclability and potential application of STLB, successive batches of CTC removal were carried out under the same experimental condition. As shown in Fig. 4c, over the course of five cycles, about 97.4 %, 97.3 %, 97.1 %, 95.7 %, and 94.0 % of CTC were removed after 90 min treatment, respectively. The slight decrease of removal efficiency might be due to partial intermediates generated during the catalytic degradation process, which might remain on the surface of STLB and even restrain further adsorption of CTC for a short time. The same phenomenon was also observed in the degradation of benzotriazole by a novel Fenton-like reaction with mesoporous Cu/MnO_2 (Zhang et al., 2016). But the overall effect was relatively small and CTC could still be quickly removed in the combined pre-adsorption and PS-AOP after five cycles of reuse. Thus, as an adsorption-enhanced persulfate activator, the STLB had good recycling performance for CTC removal.

The CTC degradation was always accompanied by TOC removal in the combined pre-adsorption and PS-AOP. Thus, the mineralization efficiency of CTC derived by the STLB was also studied and the results were provided in Fig. 4d. The mineralization efficiency was distinctly lower than the CTC removal efficiency owing to the production of many intermediates during the CTC degradation (Chen et al., 2019). By contrast, only 18.3 % of TOC was removed within 30 min of pre-adsorption. However, the TOC removal efficiency was improved rapidly with the increase of time, and about 57.1 % TOC was removed within 60 min of subsequent catalytic degradation. The result further confirmed that the mineralization of CTC was mainly due to the generation of reactive oxygen species in the catalytic degradation stage.

3.2.3. Removal mechanism of CTC in combined pre-adsorption and PS-AOP

3.2.3.1. Adsorption mechanism of the spent tea leaves-based biochar. The superior adsorption performance of STLB for CTC removal might be due to the following factors: (1) high specific surface area and hierarchical porous structure, which had been confirmed by BET analyses; (2) electrostatic attraction between STLB and CTC molecules (Text S2 and Fig. S2); (3) oxygen-containing functional groups, which had been confirmed by FTIR spectra of STLB before and after CTC adsorption (Test S3 and Fig. S3).

3.2.3.2. Activation mechanism of the spent tea leaves-based biochar. The activation of PDS by catalyst may produce some reactive oxygen species, namely $SO_4^{\cdot-}$, •OH and $^1O_2$ (Liu et al., 2020). Thus, EPR experiments with DMPO and TEMP as trapping agents were performed to identify the main reactive species in the degradation process. As depicted in Fig. 5a, no obvious signals of any free radicals or $^1O_2$ were found in the presence of PDS. However, both DMPO-OH and DMPO-SO_4 signals were observed in combined pre-adsorption and PS-AOPs derived by the STLB. When pH was increased from 3.0 to 9.0, the intensities of DMPO-OH and DMPO-SO_4 first increased and then decreased. The results indicated that the activated PDS might be dissociated to generated more reactive radicals ($SO_4^{\cdot-}$ and •OH) at pH 6.0. Additionally, the TEMP-$^1O_2$ signals (1:1:1) were also observed after PDS was added (Fig. 5b), suggesting that the active $^1O_2$ species were generated via the activation of STLB. And the intensity of TEMP adducts were similarly stronger at pH 6.0.

Numerous studies have shown that EtOH could efficiently quench both •OH and $SO_4^{\cdot-}$, whereas TBA is an effective quencher for •OH generated in solution or surface bounds. Additionally, NaN_3 could determine the existence of $^1O_2$ (Zhou et al., 2020). Thus, to further identify the contribution of reactive species on the CTC degradation, quenching tests were conducted using EtOH, TBA and NaN_3 as scavengers, respectively (Zhu et al., 2019). As could be seen from Fig. 5c, without adding any quenching agents, about 97.4 % CTC was removed within 30 min of pre-adsorption and 60 min of subsequent oxidation degradation. In the presence of TBA and EtOH, the CTC removal was decreased to 93.4 % and 82.6 %, respectively, demonstrating that both $SO_4^{\cdot-}$ and •OH co-existed in the catalytic degradation system. But the quenching effect of TBA and EtOH wasn't particularly significant, indirectly proving the presence of other reactive species. Meanwhile, NaN_3 was also dramatically able to quench the reactions, suggesting that $^1O_2$ might play an important role in the CTC degradation. Thus, the active species involving $SO_4^{\cdot-}$, •OH and $^1O_2$ were jointly responsible for the degradation and mineralization of CTC, in which $^1O_2$ might be dominant in PDS activation by using the STLB.

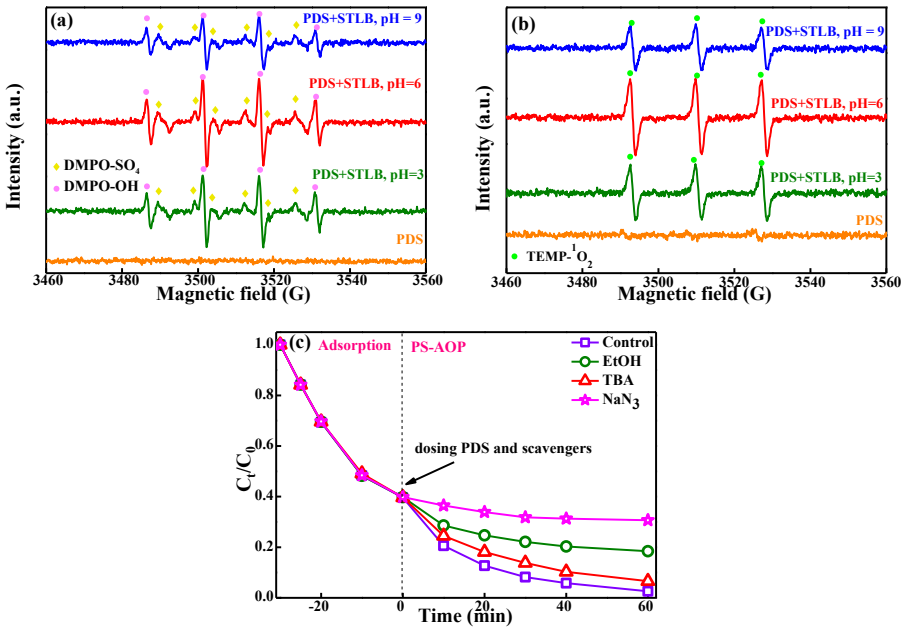

Fig. 5. EPR spectrum of species adducts trapped by DMPO (a) and TEMP (b); and (c) comparison of the CTC removal under various quenching conditions in combined pre-adsorption and PS-AOP.

3.3. 3 Removal mechanism of the spent tea leaves-based biochar

According to the above analysis, a possible mechanism of CTC removal in combined pre-adsorption and PS-AOP derived by the STLB was described in Fig. 6. The STLB provided enough active sites for CTC adsorption and PDS activation. In the pre-adsorption stage, trace amounts of CTC could be firstly adsorbed and enriched onto the surface of STLB. And then the catalytically generated reactive oxygen species rapidly degraded and mineralized the adsorbed CTC, facilitating the subsequent continuous adsorption process. Both biochar and iron in the STLB could simulate PDS to generate some active species including $SO_4^{\bullet-}$, •OH and $^1O_2$ via radical and non-radical pathways. And the detail mechanism of PDS activation over the STLB is mediated by the delocalized π-electrons and iron (Eqs. (5) - (11)) (Chen et al., 2020; Matzek et al., 2016).

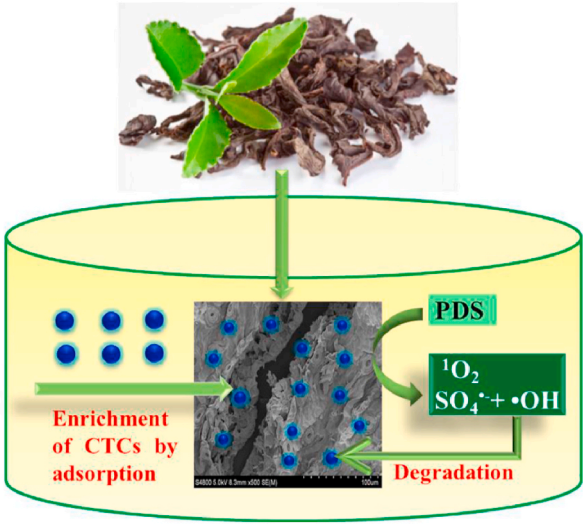

Fig. 6. Reaction mechanism of enhanced CTC removal in combined pre-adsorption and PS-AOP derived by the STLB.

$$C-\pi + S_2O_8^{2-} \rightarrow C-\pi^+ + SO_4^{2-} + SO_4^{\bullet-} \quad (5)$$

$$SO_4^{\bullet-} + H_2O \rightarrow SO_4^{2-} + \cdot OH + H^+ \quad (6)$$

$$S_2O_8^{2-} + H_2O \rightarrow HSO_5^- + HSO_4^- \quad (7)$$

$$C-\pi^+ + HSO_5^- \rightarrow C-\pi + H^+ + SO_5^{\bullet-} \quad (8)$$

$$2SO_5^{\bullet-} + H_2O \rightarrow 2HSO_4^- + 1.5\ 1O_2 \quad (9)$$

$$S_2O_8^{2-} + Fe^0 \rightarrow Fe^{2+} + 2SO_4^{2-} \quad (10)$$

$$S_2O_8^{2-} + Fe^{2+} \rightarrow Fe^{3+} + SO_4^{2-} + SO_4^{\bullet-} \quad (11)$$

4. Conclusions

Herein, a low-cost heteroatom-doped porous STLB was successfully prepared. The as-prepared STLB could firstly behave as an adsorbent for the accumulation of CTCs molecules in water, and subsequently as an efficient PDS activator for the CTC degradation. Meanwhile, the STLB itself would be regenerated, and thus recycled. The maximum adsorption capacity of STLB obtained from the Langmuir model was 627 mg g^{-1}. And nearly 97.4 % of CTC was removed within 30 min of pre-adsorption and 60 min of subsequent oxidation degradation. Due to adsorption and oxidation of radicals ($SO_4^{\bullet-}$ and •OH) and non-radical including $^1O_2$, the CTC could be quickly removed over a wide pH range of 3.0–9.0. The findings indicate the STLB has great potential as a sustainable adsorption-enhanced persulfate activator for the removal of antibiotics and other refractory organic pollutants from wastewater, especially at trace levels. The study also provided a strategy of waste control by waste and turning spent tea leave into treasure.

Credit Author Statement

Yi-Ping Chen: Conceptualization, Methodology, Data curation, Writing – original draft preparation, Funding acquisition. Chao-Hong Zheng: Methodology, Investigation, Supervision. Yao-Yi Huang: Validation, Resources. Yi-Ren Chen: Investigation, Visualization.

Declaration of competing interest

The authors declare that they have no known competing financial interests or personal relationships that could have appeared to influence the work reported in this paper.

Acknowledgments

This work was partially supported by the Natural Science Foundation of Fujian Province, China (Grant No. 2017J01713), the Science and Technology Bureau Project of Quanzhou City of China (Grant No. 2014z118).

Appendix A. Supplementary data

Supplementary data to this article can be found online at https://doi.org/10.1016/j.chemosphere.2021.131770.

References

Bsoul, A.A., Hailat, M., Abdelhay, A., Tawalbeh, M., Al-Othman, A., Al-kharabsheh, I., Al-Taani, A.A., 2021. Efficient removal of phenol compounds from water environment using Ziziphus leaves adsorbent. Sci. Total Environ. 761, 143229.

Chen, F., Wu, X.L., Yang, L., Chen, C., Lin, H., Chen, J., 2020. Efficient degradation and mineralization of antibiotics via heterogeneous activation of peroxymonosulfate by using graphene supported single-atom Cu catalyst. Chem. Eng. J. 394, 124904.

Chen, Y.P., Yang, L.M., Chen, J.P., Zheng, Y.M., 2019. Electrospun spongy zero-valent iron as excellent electro-Fenton catalyst for enhanced sulfathiazole removal by a combination of adsorption and electro-catalytic oxidation. J. Hazard Mater. 371, 576–585.

Deng, F.X., Olvera-Vargas, H., Garcia-Rodriguez, O., Zhu, Y.S., Jiang, J.Z., Qiu, S., Yang, J.X., 2019. Waste-wood-derived biochar cathode and its application in electro-Fenton for sulfathiazole treatment at alkaline pH with pyrophosphate electrolyte. J. Hazard Mater. 377, 249–258.

Ding, H.J., Wu, Y.X., Zhang, W.H., Zhong, J.Y., Lou, Q., Yang, P., Fang, Y.Y., 2017. Occurrence, distribution, and risk assessment of antibiotics in the surface water of Poyang Lake, the largest freshwater lake in China. Chemosphere 184, 137–147.

Duan, X.G., Sun, H.Q., Wang, S.B., 2018. Metal-free carbocatalysis in advanced oxidation reactions. Acc. Chem. Res. 51, 678–687.

Fan, S.S., Tang, J., Wang, Y., Li, H., Zhang, H., Tang, J., Wang, Z., Li, X.D., 2016. Biochar prepared from co-pyrolysis of municipal sewage sludge and tea waste for the adsorption of methylene blue from aqueous solutions: kinetics, isotherm, thermodynamic and mechanism. J. Mol. Liq. 220, 432–441.

Gan, L., Li, B.B., Guo, M.Y., Weng, X.L., Wang, T., Chen, Z.L., 2018. Mechanism for removing 2,4-dichlorophenol via adsorption and Fenton-like oxidation using iron-based nanoparticles. Chemosphere 206, 168–174.

Hameed, B.H., 2009. Spent tea leaves: a new non-conventional and low-cost adsorbent for removal of basic dye from aqueous solutions. J. Hazard Mater. 161, 753–759.

Hou, J., Wang, C., Mao, D.Q., Luo, Y., 2016. The occurrence and fate of tetracyclines in two pharmaceutical wastewater treatment plants of Northern China. Environ. Sci. Pollut. Res. 23, 1722–1731.

Jiang, L.L., Zhang, Y., Zhou, M.H., Liang, L., Li, K.R., 2018. Oxidation of Rhodamine B by persulfate activated with porous carbon aerogel through a non-radical mechanism. J. Hazard Mater. 358, 53–61.

Kakavandi, B., Esrafili, A., Mohseni-Bandpi, A., Jafari, A.J., Kalantary, R.R., 2014. Magnetic Fe_3O_4@C nanoparticles as adsorbents for removal of amoxicillin from aqueous solution. Water Sci. Technol. 69 (1), 147–155.

Karak, T., Paul, R.K., Kutu, F.R., Mehra, A., Khare, P., Dutta, A.K., Bora, K., Boruah, R.K., 2017. Comparative assessment of Copper, Iron, and Zinc contents in selected Indian (Assam) and South African (Thohoyandou) tea (Camellia sinensis L.) samples and their infusion: a quest for health risks to consumer. Biol. Trace Elem. Res. 175, 475–487.

Kumar, P., Sengupta, A., Deb, A.K.S., Dasgupta, K., Ali, S.M., 2016. Sorption behaviour of Pu^{4+} and PuO_2^{2+} on amido amine-functionalized carbon nanotubes: experimental and computational study. RSC Adv. 6, 107011.

Liu, Q., Zhong, L.B., Zhao, Q.B., Frear, C., Zheng, Y.M., 2015. Synthesis of Fe_3O_4/Polyacrylonitrile composite electrospun nanofiber mat for effective adsorption of Tetracycline. ACS Appl. Mater. Interfaces 7, 14573–14583.

Liu, Y., Miao, W., Fang, X., Tang, Y.L., Wu, D.L., Mao, S., 2020. MOF-derived metal-free N-doped porous carbon mediated peroxydisulfate activation via radical and non-radical pathways: role of graphitic N and C-O. Chem. Eng. J. 380, 122584.

Li, W., Li, Y.X., Zhang, D.Y., Lan, Y.Q., Guo, J., 2020. CuO-Co_3O_4@CeO_2 as a heterogeneous catalyst for efficient degradation of 2,4-dichlorophenoxyacetic acid by peroxymonosulfate. J. Hazard Mater. 381, 121209.

Li, Y., Gong, Y., Zhao, H., Gu, J., Wang, Z., He, X., 2020. Enhancement of chlortetracycline biodegradation with Trichoderma harzianum LJ245 and its spore-producing mutants using co-metabolism. Biodegradation 31, 265–273.

Mandal, S., Pu, S.Y., Shangguan, L.X., Liu, S.B., Ma, H., Adhikari, S., Hou, D.Y., 2020. Synergistic construction of green tea biochar supported nZVI for immobilization of lead in soil: a mechanistic investigation. Environ. Int. 135, 105374.

Matzek, L.W., Carter, K.E., 2016. Activated persulfate for organic chemical degradation: a review. Chemosphere 151, 178–188.

Ng, I.S., Wu, X., Yang, X., Xie, Y., Lu, Y., Chen, C., 2013. Synergistic effect of Trichoderma reesei cellulases on agricultural tea waste for adsorption of heavy metal Cr(VI). Bioresour. Technol. 145, 297–301.

Oh, W.D., Dong, Z.L., Lim, T.T., 2016. Generation of sulfate radical through heterogeneous catalysis for organic contaminants removal: current development, challenges and prospects. Appl. Catal., B 194, 169–201.

Ouda, M., Kadadou, D., Swaidan, B., Al-Othman, A., Al-Asheh, S., Banat, F., Hasan, S.W., 2021. Emerging contaminants in the water bodies of the Middle East and North Africa (MENA): a critical review. Sci. Total Environ. 754, 142177.

Peiris, C., Gunatilake, S.R., Mlsna, T.E., Mohan, D., Vithanage, M., 2017. Biochar based removal of antibiotic sulfonamides and tetracyclines in aquatic environments: a critical review. Bioresour. Technol. 246, 150–159.

Qalyoubi, L.Y., Al-Othman, A., Al-Asheh, S., 2021. Recent progress and challenges of adsorptive membranes for the removal of pollutants from wastewater. Part II: environmental applications. Case Studies in Chemical and Environmental Engineering 3, 100102.

Razmovski, R., Šćiban, M., 2008. Biosorption of Cr(VI) and Cu(II) by waste tea fungal biomass. Ecol. Eng. 34 (2), 179–186.

Wang, J.C., Ma, R.G., Zhou, Z.Z., Liu, G.H., Liu, Q., 2015. Magnesiothermic synthesis of sulfur-doped graphene as an efficient metal-free electrocatalyst for oxygen reduction. Sci. Rep. 5, 9304.

Wang, H.Z., Guo, W.Q., Liu, B.H., Wu, Q.L., Luo, H.C., Zhao, Q., Si, Q.S., Sseguya, F., Ren, N.Q., 2019. Edge-nitrogenated biochar for efficient peroxydisulfate activation: an electron transfer mechanism. Water Res. 160, 405–414.

Wang, H.Z., Guo, W.Q., Liu, B.H., Si, Q.S., Luo, H.C., Zhao, Q., Ren, N.Q., 2020. Sludge-derived biochar as efficient persulfate activators: sulfurization-induced electronic structure modulation and disparate nonradical mechanisms. Appl. Catal., B 279, 119361.

Wan, Z.H., Sun, Y.Q., Tsang, D.C.W., Khan, e., Yip, A.C.K., Ng, Y.H., Rinklebe, J., Ok, Y. S., 2020. Customised fabrication of nitrogen-doped biochar for environmental and energy applications. Chem. Eng. J. 401, 126136.

Worasuwannarak, N., Nakagawa, H., Miura, K., 2002. Effect of pre-oxidation at low temperature on the carbonization behavior of coal. Fuel 81, 1477–1484.

Yu, J.F., Feng, H.P., Tang, L., Pang, Y., Zeng, G.M., Lu, Y., Dong, H.R., Wang, J.J., Liu, Y. N., Feng, C.Y., Wang, J.J., Peng, B., Ye, S.J., 2020. Metal-free carbon materials for persulfate-based advanced oxidation process: microstructure, property and tailoring. Prog. Mater. Sci. 111, 100654.

Yu, J.F., Feng, H.P., Tang, L., Pang, Y., Wang, J.J., Zou, J.J., Xie, Q.Q., Liu, Y.N., Feng, C. Y., Wang, J.J., 2021. Insight into the key factors in fast adsorption of organic pollutants by hierarchical porous biochar. J. Hazard Mater. 403, 123610.

Zhang, Y.T., Liu, C., Xu, B.B., Qia, F., Chu, W., 2016. Degradation of benzotriazole by a novel Fenton-like reaction with mesoporous Cu/MnO_2: combination of adsorption and catalysis oxidation. Appl. Catal., B 199, 447–457.

Zhao, Q.X., Mao, Q.M., Zhou, Y.Y., Wei, J.H., Liu, X.C., Yang, J.Y., Luo, L., Zhang, J.C., Chen, H., Chen, H.B., Tang, L., 2017. Metal-free carbon materials-catalyzed sulfate radical-based advanced oxidation processes: a review on heterogeneous catalysts and applications. Chemosphere 189, 224–238.

Zhu, S.S., Li, X.J., Kang, J., Duan, X.G., Wang, S.B., 2019. Persulfate activation on crystallographic manganese oxides: mechanism of singlet oxygen evolution for nonradical selective degradation of aqueous contaminants. Environ. Sci. Technol. 53, 307–315.